HOKKAIDO UNIVERSITY

| | |
|---|---|
| Title | Synthesis, crystal structures and magnetic properties of fluorite-related compounds Ce3MO7 (M = Nb, Ta) |
| Author(s) | Inabayashi, Masaki; Doi, Yoshihiro; Wakeshima, Makoto; Hinatsu, Yukio |
| Citation | Journal of solid state chemistry, 254, 150-154<br>https://doi.org/10.1016/j.jssc.2017.07.022 |
| Issue Date | 2017-10 |
| Doc URL | http://hdl.handle.net/2115/75621 |
| Rights | ©2017. This manuscript version is made available under the CC-BY-NC-ND 4.0 license<br>https://creativecommons.org/licenses/by-nc-nd/4.0/ |
| Rights(URL) | https://creativecommons.org/licenses/by-nc-nd/4.0/ |
| Type | article (author version) |
| File Information | Ce3MO7.pdf |

Instructions for use

Hokkaido University Collection of Scholarly and Academic Papers : HUSCAP

# Synthesis, Crystal Structures and Magnetic Properties of Fluorite-related Compounds $Ce_3MO_7$ ($M$ = Nb, Ta)

Masaki Inabayashi, Yoshihiro Doi, Makoto Wakeshima and Yukio Hinatsu

Division of Chemistry, Graduate School of Science, Hokkaido University, Sapporo 060-0810, Japan

Key-words: Cerium; Niobium, Tantalum, Oxides; Crystal structure; Magnetic properties.

**Abstract**

Ternary oxides $Ce_3NbO_7$ and $Ce_3TaO_7$ were successfully synthesized by the solid state reaction under flowing hydrogen atmosphere. The structures were determined by the powder X-ray diffraction. Both the compounds were crystallized in the orthorhombic space groups *Pnma* (for $Ce_3NbO_7$) and *Cmcm* (for $Ce_3TaO_7$).

Both the structures have similar features: two kinds of infinite chains formed by corner-sharing $NbO_6$ ($TaO_6$) octahedra and edge-sharing $Ce(1)O_8$ cubes, the slabs consisting of alternate chains, and 7-coordinated Ce(2) ions existing between the slabs. In the structure of $Ce_3NbO_7$, the $NbO_6$ octahedra running along the *a*-axis are titled towards the 0 0 1 direction, while in the $Ce_3TaO_7$ structure, the $TaO_6$ octahedra running along the *c*-axis are titled towards the 0 1 0 direction.

Magnetic susceptibility measurements for $Ce_3NbO_7$ and $Ce_3TaO_7$ show that both compounds are paramagnetic down to 1.8 K, and confirm that the Ce ion is in the trivalent state. From specific heat ($C_p$) measurements, a rapid increase of $C_p/T$ has been observed below 3 K for both the compounds, indicating the onset of magnetic ordering between $Ce^{3+}$ ions at further lower temperatures.

## 1. Introduction

It is well known that oxides containing rare earth elements show a variety of magnetic properties due to the behavior of unpaired 4f electrons. When the rare ions are arrayed in a structurally characteristic manner, interesting magnetic behavior has been often found.

Here, we focus our attention on compounds with the general formula $Ln_3MO_7$, where *Ln* is a rare earth and *M* is the 4*d* or 5*d* transition metal. Rossell determined first the parent structure of this family of compounds, $La_3NbO_7$ [1]. These compound have a characteristic defect-fluorite structure. The relationship to the fluorite structure is as follows. The fluorite unit cell for oxides has the composition $M^{4+}{}_4O_8$. If the four tetravalent metal ions are replaced by three trivalent ions (*Ln*) and one pentavalent ion (*M*), one oxide vacancy is formed per fluorite cell. Due to significant differences in radii between the $Ln^{3+}$ and $M^{5+}$ ions, cation ordering occurs on the metal sites and the oxide-vacancy orders on the anion sites. The $M^{5+}$ ion is coordinated with six oxygen ions, forming an $MO_6$ octahedron. These octahedra share corners forming one-dimensional chains which are oriented along the *c*-axis. One-third of the *Ln* ions are coordinated by eight oxygen ions and the $LnO_8$ cubes also form a one-dimensional chain through edge-sharing.

Many studies have been performed, due to this unique crystal structure and possible related magnetic properties for $Ln_3MO_7$ compounds (*M* = Mo [2-4], Ru [5-20], Re [21-24], Os [14, 25-27], and Ir [28-31]). Since the trivalent state is a stable oxidation state common to all rare earth ions, it is expected to form $Ln_3MO_7$ compounds from *Ln* = La to Lu. However, a

molybdate $CeMoO_7$ is the only cerium-containing compound [32]. One reason for this is that in addition to the trivalent state, the tetravalent state is also stable for cerium ions.

In this study, we challenged to obtain cerium-containing $Ln_3MO_7$ compounds for $M$ = Nb, Ta, and have prepared $Ce_3NbO_7$ and $Ce_3TaO_7$ for the first time. Through X-ray diffraction measurements, their structures were determined, and magnetic susceptibility and specific heat measurements were performed from 1.8 to 300 K to study their magnetic properties.

## 2. Experimental

### *2.1. Sample Preparation*

Two $Ce_3MO_7$ compounds ($M$ = Nb, Ta) could be prepared by the solid state reaction in flowing hydrogen atmosphere. As starting materials, cerium dioxide $CeO_2$, niobium oxide $Nb_2O_5$ and tantalum oxide $Ta_2O_5$ were used. They were weighed in an appropriate metal ratio and the mixtures were ground in an agate mortar. The mixtures were pressed into pellets and then heated in a flow of $H_2$ gas at 1300 °C for 12 h. After cooling to room temperature, the pellets were crushed, re-pressed into pellets, and reheated in the same conditions. These procedures were repeated three times.

### *2.2. X-ray Diffraction Analysis*

Powder X-ray diffraction profiles were measured using a Rigaku Multi-Flex diffractometer with Cu-$K\alpha$ radiation ($\lambda$ = 1.5406 Å) equipped with a curved graphite monochromator. The data were collected by step-scanning in the angle range of $10° \leq 2\theta \leq 120°$ at a $2\theta$ step-size of 0.02°.

The X-ray diffraction data were analyzed by the Rietveld technique, using the programs RIETAN-FP [33], and the crystal structure was drawn by using the VESTA program [34].

*2.3. TG-DTA Measurements*

To check the thermal stability of the specimens, thermogravimetric and differential thermal analysis (TG-DTA) measurements were performed with a TG-DTA 2000S (Mac Science) over the temperature range of 300-800 K with a heating rate of 5 K $min^{-1}$ in a flow of oxygen gas. In this measurement, $\alpha$-$Al_2O_3$ was used as a standard material.

*2.4. Magnetic Susceptibility Measurements*

The temperature-dependence of the magnetic susceptibility was measured in an applied field of 0.1T over the temperature range of 1.8K ≤ $T$ ≤ 300K, using a SQUID magnetometer (Quantum Design, MPMS5S). The susceptibility measurements were performed under both zero-field-cooled (ZFC) and field-cooled (FC) conditions. The former was measured upon heating the sample to 300 K under the applied magnetic field of 0.1 T after zero-field cooling to 1.8 K. The latter was measured upon cooling the sample from 300 to 1.8 K at 0.1 T.

*2.5. Specific Heat Measurements*

The specific heat measurements were carried out using a relaxation technique with a commercial physical property measurement system (Quantum Design, PPMS) in the temperature range of 1.8K ≤ $T$ ≤ 300K. The pelletized sample (~10 mg) was mounted on a thin alumina plate with Apiezon N-grease for better thermal contact.

## 3. Results and Discussion

*3.1. Synthesis and crystal structure*

In this study, we have synthesized, for the first time, two compounds $Ce_3NbO_7$ and $Ce_3TaO_7$ under heating conditions in a flow of $H_2$ gas. For compounds containing *M* = Ru, Ir, Os, Re, it will be difficult to obtain $Ce_3MO_7$ compounds in the same preparation conditions, because these transition metals are more easily reduced than cerium. Figure 1 (a) shows the X-ray diffraction profile of $Ce_3TaO_7$. Crystal structures for $La_3TaO_7$ and $Pr_3TaO_7$ have been reported to be well described in the orthorhombic space group *Cmcm* [35]. The diffraction patters are similar to that for the fluorite structure and all reflections appeared to be consistent with the C-centered conditions, $h + k = 2n$, and $h$ 0 $l$ reflections with odd $l$ are absent. We have analyzed the X-ray diffraction profiles with the same space group *Cmcm*. All the reflections observed could be successfully indexed. The crystallographic data determined for $Ce_3TaO_7$ are listed in Table 1.

Figure 1 (b) shows the X-ray diffraction profile of $Ce_3NbO_7$. We tried to analyze the X-ray diffraction data with the *Cmcm* model, but some reflection peaks cannot be explained from the extinction conditions (for example, the peak at $2\theta \sim 27.5°$ which is indexed to be 1 1 2). Previously, $La_3NbO_7$, $Pr_3NbO_7$ and $Nd_3NbO_7$ were reported to be crystallized in the orthorhombic space group *Pnma* [36]. Then, we performed Rietveld analysis for the X-ray diffraction data on $Ce_3NbO_7$ with the *Pnma* model. All the reflections observed of $Ce_3NbO_7$ could be successfully indexed with the same space group. The structural parameters determined for $Ce_3NbO_7$ are listed in Table 2.

The crystal structures for $Ce_3TaO_7$ (*Cmcm*) and $Ce_3NbO_7$ (*Pnma*) are illustrated in Fig. 2. Both the structures have similar features: two kinds of infinite chains formed by corner-sharing $TaO_6$ ($NbO_6$) octahedra and edge-sharing $Ce(1)O_8$ cubes, the slabs consisting of alternate chains, and 7-coordinated Ce(2) ions existing between the slabs. As depicted in Fig.3, the $TaO_6$ octahedra running along the *c*-axis are titled towards the 0 1 0 direction in the structure of $Ce_3TaO_7$ and the Ta-O-Ta angle is 160.4°, while in the $Ce_3NbO_7$ structure, the $NbO_6$ octahedra running along the *a*-axis are titled towards the 0 0 1 direction and the Nb-O-Nb angle is 153.9°.

Figures 4(a) and (b) show the variation of lattice parameters for $Ln_3TaO_7$ (*Ln* = La – Nd) and $Ln_3NbO_7$ (*Ln* = La – Nd) against the ionic radii of the 8-coordinate $Ln^{3+}$ ions [37], respectively. The lattice parameter data for $Ln_3TaO_7$ (*Ln* = La, Pr, Nd) and $Ln_3NbO_7$ (*Ln* = La, Pr, Nd) were obtained from references [35, 36]. The unit cell is orthorhombic with dimensions $a \sim 2a_f$, $b \sim \sqrt{2}a_f$, $c \sim \sqrt{2}a_f$ for $Ln_3TaO_7$, and $a \sim \sqrt{2}a_f$, $b \sim 2a_f$, $c \sim \sqrt{2}a_f$ for $Ln_3NbO_7$ ($a_f$ : the unit cell of the fluorite structure). For comparison, all the data are converted to $\sqrt{2}a_f$. The lattice parameters tend to increase smoothly with the ionic radius of $Ln^{3+}$ ions. This result also indicates that all the rare earth ions are in the trivalent state.

*3.2. Thermal stability*

In order to investigate the thermal stability of $Ce_3MO_7$ (*M* = Nb and Ta), the TG-DTA measurements were performed in a flow of $O_2$ gas (Fig. 5). In both data, the sample weight begins to increase at ~450 K and reaches a constant value (+3.5 % for *M* = Nb and +3.1 % for Ta) at 600 K. The DTA curve also shows a broad exothermic peak between these temperatures.

The increments are close to 3.8 and 3.4 %, respectively, which are calculated by assuming that all the trivalent Ce ions are oxidized to the tetravalent state. In the XRD patterns for the samples after TG-DTA measurements, the $Ce_3MO_7$ phase was not detected and the two kinds of fluorite-like phases were observed. These facts suggest that the $Ce_3MO_7$ compounds are easily oxidized and decomposed by heating in an $O_2$ atmosphere.

*3.3. Magnetic properties*

Figure 6 depicts the temperature dependence of the magnetic susceptibility for $Ce_3TaO_7$ in the temperature range between 1.8 and 300 K. Since the electronic configuration of $Ce^{3+}$ ion is [Xe]$4f^1$ ([Xe]: xenon electronic core), magnetic interactions between $Ce^{3+}$ ions are expected. However, no magnetic ordering has been observed down to 1.8 K. The reciprocal magnetic susceptibility vs. temperature curve has been also shown in the same figure. In the high temperature region, the Curie-Weiss law fitting was applied to the temperature dependence of the susceptibility. The effective magnetic moment and the Weiss constant for $Ce_3TaO_7$ were obtained to be 2.95 $\mu_B$ and -12.6 K, respectively. Since $Ta^{5+}$ ions do not contribute to the paramagnetic behavior of $Ce_3TaO_7$, the effective magnetic moment per mole of $Ce^{3+}$ ions is calculated to be 1.71 $\mu_B$. Since the ground state of $Ce^{3+}$ is $^2F_{5/2}$, the effective magnetic moment for the free $Ce^{3+}$ ion is 2.54 $\mu_B$, i.e., the experimental magnetic moment is smaller than the free ion value. This result means that the smaller effective magnetic moment of $Ce^{3+}$ ion is due to the effect of crystal field [38]. The same results have been reported for $Pr^{4+}$-containing compounds [39]. The electronic configuration of $Pr^{4+}$ is the same as that of $Ce^{3+}$.

For $Ce_3NbO_7$, its temperature dependence of the magnetic susceptibility and the reciprocal

magnetic susceptibility is shown in Fig. 7. No magnetic ordering has been observed down to 1.8 K. By applying the Curie-Weiss law to the reciprocal susceptibility vs. temperature curve, the effective magnetic moment and the Weiss constant for $Ce_3NbO_7$ were determined to be 3.06 $\mu_B$ and -13.6 K. $Nb^{5+}$ ions are also diamagnetic, and they do not contribute to the magnetic behavior of $Ce_3NbO_7$. Therefore, the effective magnetic moment per mole of $Ce^{3+}$ ions is calculated to be 1.77 $\mu_B$. Smaller effective magnetic moment of $Ce^{3+}$ ion compared with the free ion value is due to the crystal field effect on the $Ce^{3+}$ ions.

In order to clarify the possibility of magnetic ordering of $Ce^{3+}$ magnetic moments at low temperatures, the specific heat ($C_p$) measurements were performed. Figures 8 (a) and (b) depict the temperature dependence of $C_p/T$ for $Ce_3NbO_7$ and $Ce_3TaO_7$, respectively. Both the compounds show a rapid increasing of $C_p/T$ below 3 K, indicating the onset of magnetic ordering at further lower temperatures. It may be antiferromagnetic, because the Weiss constants are negative.

## Summary

Ternary oxides $Ce_3NbO_7$ and $Ce_3TaO_7$ were synthesized by the solid state reaction. Both the compounds were crystallized in the orthorhombic space groups *Pnma* (for $Ce_3NbO_7$) and *Cmcm* (for $Ce_3TaO_7$). Magnetic susceptibility measurements for $Ce_3NbO_7$ and $Ce_3TaO_7$ confirm that the Ce ions are in the trivalent state.

## References

[1] J. E. Greedan, N. P. Raju, A. Wegner, P. Gougeon, and J. Padiou, *J. Solid State Chem*., **129**, 320-327 (1997).

[2] J. E. Greedan, N. P. Raju, A. Wegner, P. Gougeon, and J. Padiou, *J. Solid State Chem*., **129**, 320-327 (1997).

[3] H. Nishimine, M. Wakeshima, and Y. Hinatsu, *J. Solid State Chem*., **178**, 1221-1229 (2005).

[4] M. Wakeshima and Y. Hinatsu, *J. Solid State Chem*., **183**, 2681-2688 (2010).

[5] F. P. F. van Berkel and D. J. W. IJdo, *Mater. Res. Bull*., **21**, 1103-1106 (1986).

[6] W. A. Groen, F. P. F. van Berkel, and D. J. W. IJdo, *Acta Crystallogr*. Sec. **C 43**, 2262-2264 (1986).

[7] A. Kahn-Harari, L. Mazerrolles, D. Michel, and F. Robert, *J. Solid State Chem*., **116**, 103-106 (1995).

[8] P. Khalifah, R. W. Erwin , J. W. Lynn, Q. Huang, B. Batlogg, and R. J. Cava, *Phys. Rev.*, **B 60**, 9573-9578 (1999).

[9] F. Wiss, N. P. Raju, A. S. Wills, and J. E. Greedan, *Inter. J. Inorg. Mater.*, **2**, 53-59 (2000).

[10] B.P.Bontchev, A.J.Jacobson, M.M.Gospodinov, V. Skumryev, V. N. Popov, B. Lorenz, R. L. Meng, A. P. Litvinchuk, and M.N. Iliev, *Phys. Rev*. **B. 62**, 12235-12240 (2000).

[11] D. Harada and Y. Hinatsu, *J. Solid State Chem*., **158**, 245-253 (2001).

[12] D. Harada, Y. Hinatsu, and Y. Ishii, *J. Phys.: Condens. Matter*, **13**, 10825-10836 (2001).

[13] D. Harada and Y. Hinatsu, *J. Solid State Chem*., **164**, 163-168 (2002).

[14] R. Lam, F. Wiss, and J. E. Greedan, *J. Solid State Chem.* **167**, 182-187 (2002).

[15] Z. X. Zhou, G. Cao, S. McCall, J. E. Crow, R. P. Guertin, C. H. Mielke, and D. G. Rickel,

*Philosophical Magazine*, **82**, 1401-1412 (2002).

[16] W. R. Gemmill, M. D. Smith, and H-C, zur Loye, *Inorg. Chem*., **43**, 4254-4261 (2004).

[17] N. Ishizawa, K. Hiraga, D. du Boulay, H. Hibino, T. Ida, and S. Oishi, *Acta Cryst*., **E62**, i13-i16 (2006).

[18] Y. Hinatsu and Y. Doi, *J. Solid State Chem.*, **220**, 22-27 (2014).

[19] Y. Hinatsu and Y. Doi, *J. Solid State Chem.*, **239**, 214-219 (2016).

[20] M. Inabayashi, Y. Doi, M. Wakeshima, and Y. Hinatsu, *J. Solid State Chem.*, **250**, 100-106 (2017).

[21] G. Wltschek, H. Paulus, I. Svoboda, H. Ehrenberg, and H. Fuess, *J. Solid State Chem*. **125**, 1-4 (1996).

[22] R. Lam, T. Langet, and J. E. Greedan, *J. Solid State Chem*. **171**, 317-323 (2002).

[23] Y. Hinatsu, M. Wakeshima, N. Kawabuchi, and N. Taira, *J. Alloys Compd*., **374**, 79-83 (2004).

[24] M. Wakeshima and Y. Hinatsu, *J. Solid State Chem*., **179**, 3575-3581 (2006).

[25] J. R. Plaisier, R. J. Drost, and D. J. W. IJdo, *J. Solid State Chem.* **169**, 189-198 (2002).

[26] W. R. Gemmill, M. D. Smith, Y. A. Mozharivsky, G. J. Miller, and H-C, zur Loye, *Inorg. Chem.*, **44**, 7047-7055 (2005).

[27] Y. Hinatsu and Y. Doi, *J. Solid State Chem.*, **198**, 176-185 (2013).

[28] J. F. Vente and D. J. W. IJdo, *Mater. Res. Bull.*, **26**, 1255-1262 (1991).

[29] T. Fennell, S. T. Bramwell, and M. A. Green, *Can. J. Phys.*, **79**, 1415-1419 (2001).

[30] H. Nishimine, M. Wakeshima, and Y. Hinatsu, *J. Solid State Chem*., **177**, 739-744 (2004).

[31] Y. Hinatsu, Y. Doi, H. Nishimine, M. Wakeshima, and M. Sato, *J. Alloys Compd*., **488**, 541-545 (2009).

[32] P. Gall and P. Gougeon, *J. Solid State Chem*., **182**, 1035-1039 (2009).

[33] F. Izumi and K. Momma, *Solid State Phenom.*, **130**, 15-20 (2007).

[34] K. Momma and F. Izumi, *Appl. Crystallogr*., **41**, 653-658 (2008).

[35] M. Wakeshima, H. Nishimine, and Y. Hinatsu, *J. Phys.: Condens. Matter*, **16**, 4103-4120 (2004).

[36] Y. Doi, Y. Harada, and Y. Hinatsu, *J. Solid State Chem.*, **182**, 709-715 (2009).

[37] R. D. Shannon, *Acta Cryst*., **A32**, 751-767 (1976).

[38] R. L. Carlin, “Magnetochemistry”, Springer-Verlag, Berlin, 1986.

[39] Y. Hinatsu and N. Edelstein, *J. Solid State Chem.*, **112**, 53-57 (1994).

## Figure captions

Fig. 1 Powder x-ray diffraction profiles for (a) $Ce_3TaO_7$ and (b) $Ce_3NbO_7$. The calculated and observed profiles are shown on the top solid line and cross markers, respectively. The vertical marks in the middle show positions calculated for Bragg reflections. The lower trace is a plot of the difference between calculated and observed intensities. The inset of (b) shows the comparison between two structural models; the solid line on the top represents the calculated profile for the *Pnma* model. An arrow shows the diffraction line which can be explained only by the *Pnma* model.

Fig. 2. **a**: Crystal structure for $Ce_3TaO_7$ (space group: *Cmcm*) and **b**: that for $Ce_3NbO_7$ (space group: *Pnma*).

Fig. 3. **a**: Structure for $Ce_3TaO_7$ viewed from the [1 0 0] direction and **b**: that for $Ce_3NbO_7$ viewed from the [0 1 0] direction.

Fig. 4. Variation of lattice parameters for (a) $Ln_3TaO_7$ and (b) $Ln_3NbO_7$ compounds with ionic radii of 8-coordinated $Ln^{3+}$ ions.

Fig. 5. Temperature dependence of the TG (black line) and DTA (red line) for (a) $Ce_3NbO_7$ and (b) $Ce_3TaO_7$.

Fig. 6. Temperature dependences of magnetic susceptibility and reciprocal magnetic susceptibility for $Ce_3TaO_7$ in the temperature range between 1.8 and 300 K. The solid line is the Curie-Weiss fitting.

Fig. 7. Temperature dependences of magnetic susceptibility and reciprocal magnetic susceptibility for $Ce_3NbO_7$ in the temperature range between 1.8 and 300 K. The solid

line is the Curie-Weiss fitting.

Fig. 8. Temperature dependence of specific heat divided by temperature ($C_p/T$) for (a) $Ce_3NbO_7$ and (b) $Ce_3TaO_7$.

Table 1 Structural parameters for $Ce_3TaO_7$.

| Atom | Site | $x$ | $y$ | $z$ | $B$ /Å$^{2\,a}$ |
|---|---|---|---|---|---|
| Ce(1) | 4a | 0 | 0 | 0 | 0.44(7) |
| Ce(2) | 8g | 0.228(3) | 0.294(3) | 1/4 | 0.44 |
| Ta | 4b | 0 | 1/2 | 0 | 0.31(5) |
| O(1) | 16h | 0.123(9) | 0.317(8) | -0.031(3) | 0.48(2) |
| O(2) | 8g | 0.131(2) | 0.027(2) | 1/4 | 0.48 |
| O(3) | 4c | 0 | 0.456(8) | 1/4 | 0.48 |

*Note.* Space group *Cmcm* (No. 63); $a$ = 11.0514(8) Å, $b$ = 7.5668(5) Å, $c$ = 7.7153(4) Å, $V$ = 645.19(5) Å$^3$, $R_{wp}$ = 11.31 %, $R_B$ = 2.41 %, $R_e$ = 9.41 %, where $R_{wp} = \left[ \sum_i w_i \left( y_i - f_i(\boldsymbol{x}) \right)^2 / \sum_i w_i {y_i}^2 \right]^{1/2}$, $R_B = \sum_K \left| I_O(\boldsymbol{h}_K) - I(\boldsymbol{h}_K) \right| / \sum_K I_O(\boldsymbol{h}_K)$, and $R_e = \left[ (N-P) / \sum_i w_i {y_i}^2 \right]^{1/2}$.

a: For the same ions, $B$ values were fixed to be equal.

Table 2 Structural parameters for $Ce_3NbO_7$.

| Atom | Site | *x* | *y* | *z* | *B* / Å$^{2\,a}$ |
|---|---|---|---|---|---|
| Ce(1) | 4*c* | 0.004(1) | 1/4 | 0.760(7) | 0.50(2) |
| Ce(2) | 8*d* | 0.249(8) | 0.477(2) | 0.453(4) | 0.50 |
| Nb | 4*c* | 0.005(5) | 1/4 | 0.251(4) | 0.20(7) |
| O(1) | 8*d* | -0.026(3) | 0.378(9) | 0.437(1) | 0.45(5) |
| O(2) | 8*d* | -0.043(9) | 0.873(2) | -0.062(9) | 0.45 |
| O(3) | 8*d* | 0.263(6) | 0.377(9) | 0.725(1) | 0.45 |
| O(4) | 4*c* | 0.264(3) | 1/4 | 0.309(8) | 0.45 |

*Note.* Space group *Pnma* (No. 62);*a* = 7.7123(9) Å, *b* = 11.0413(1) Å, *c* = 7.5510(5) Å, *V* = 643.00(8) Å$^3$, $R_{wp}$ = 13.84 %, $R_B$ = 2.36 %, $R_e$ = 12.07 %.

a: For the same ions, *B* values were fixed to be equal.

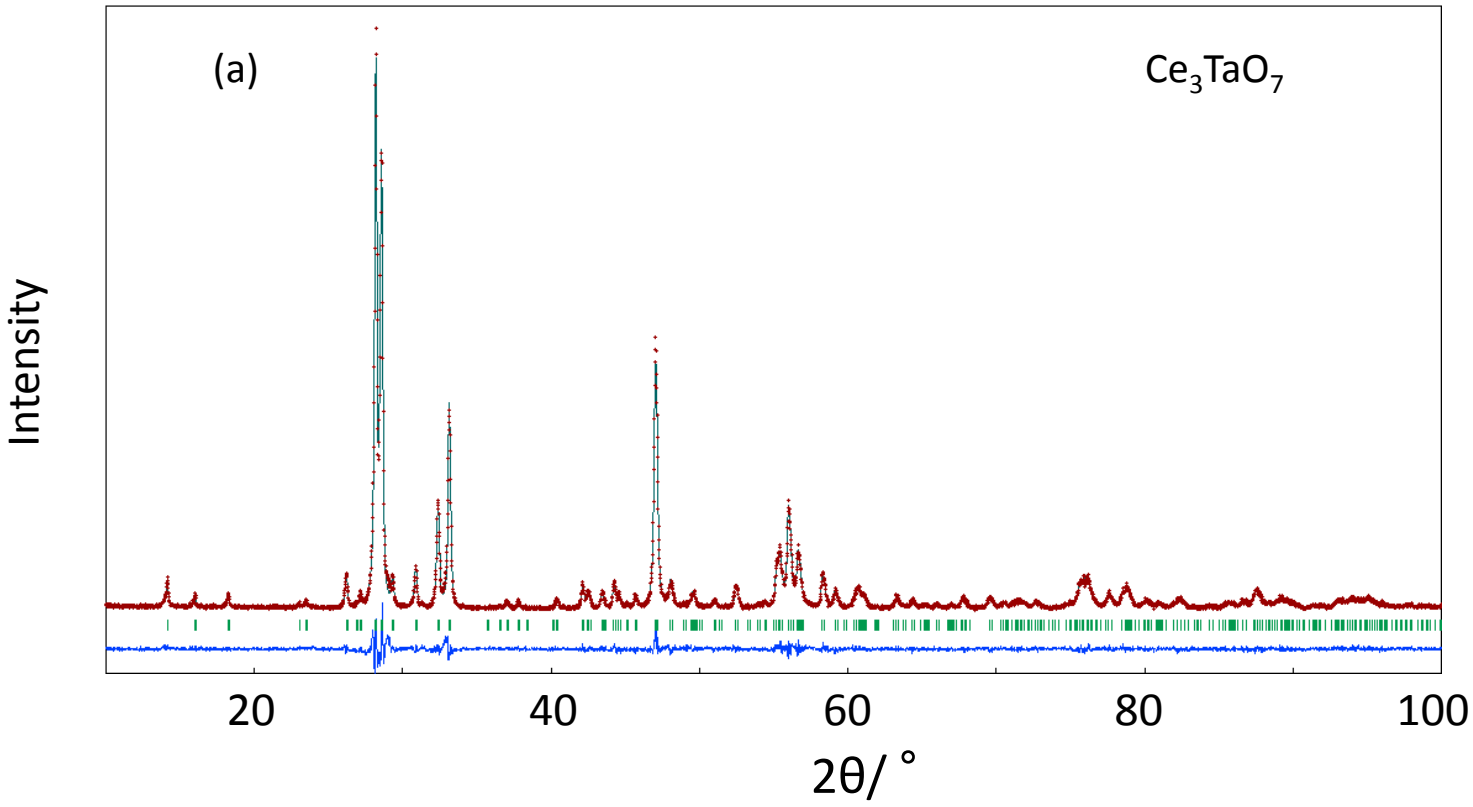


Fig.1(a)

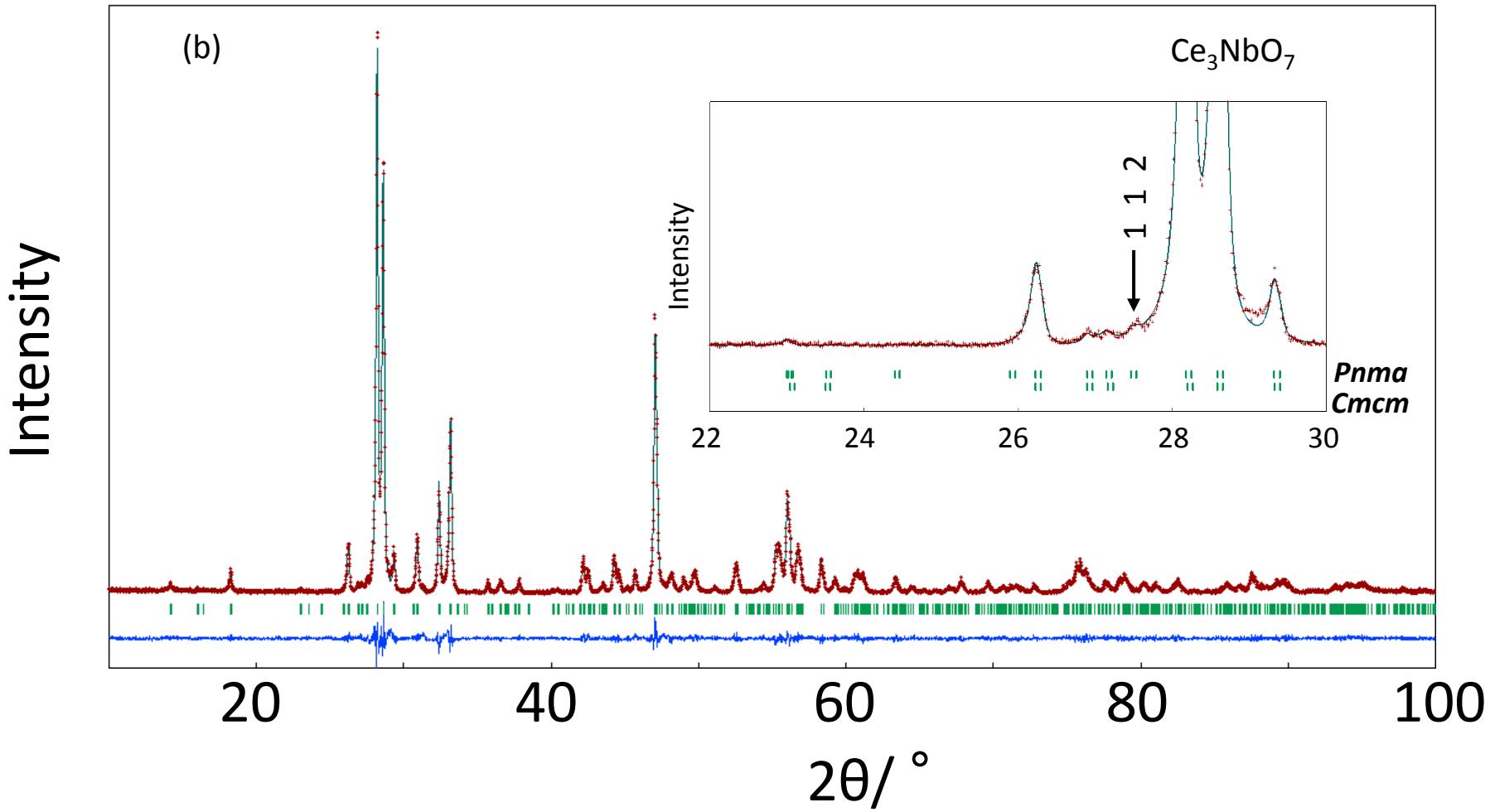
(b)
$Ce_3NbO_7$
Intensity
1 1 2
Intensity
22
24
26
28
30
Pnma
Cmcm
20
40
60
80
100
2θ/ °

Fig.1(b)

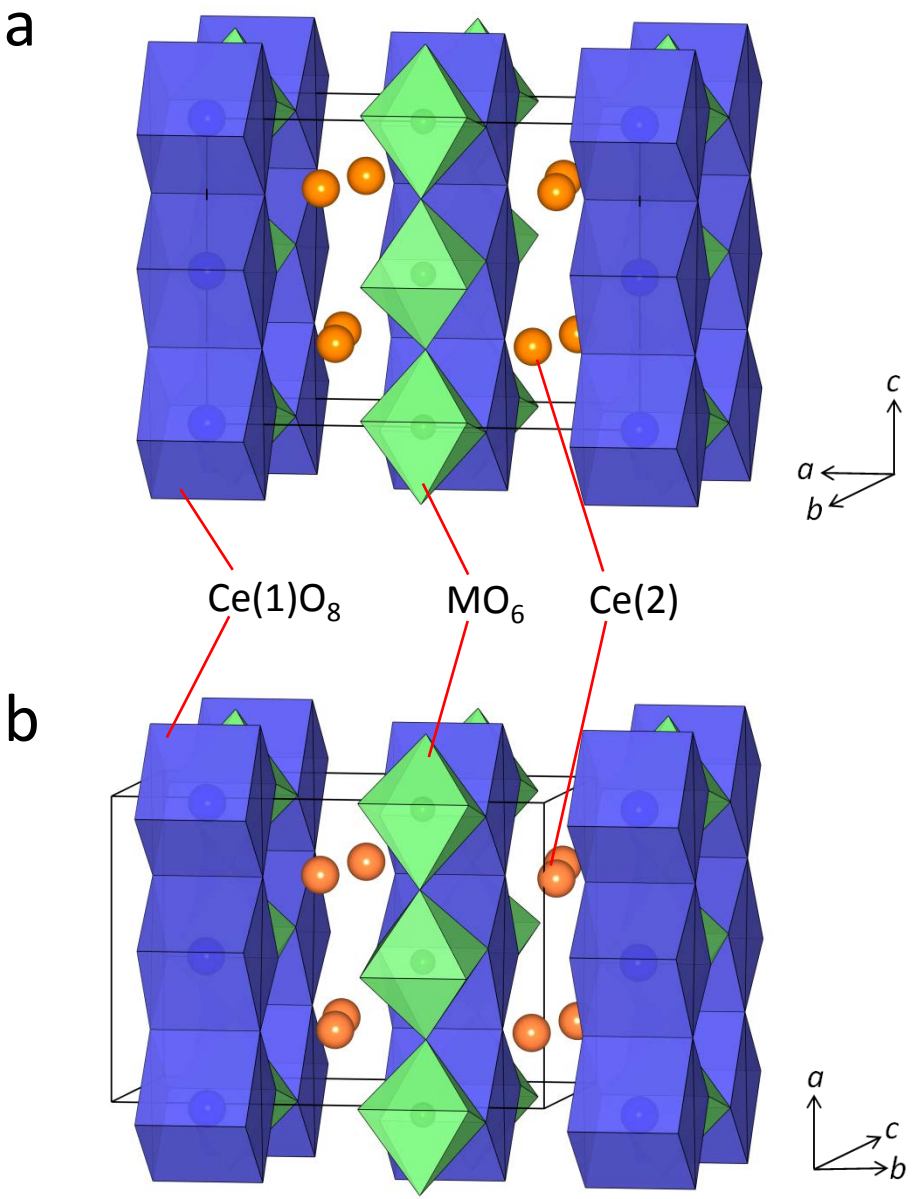


Fig.2

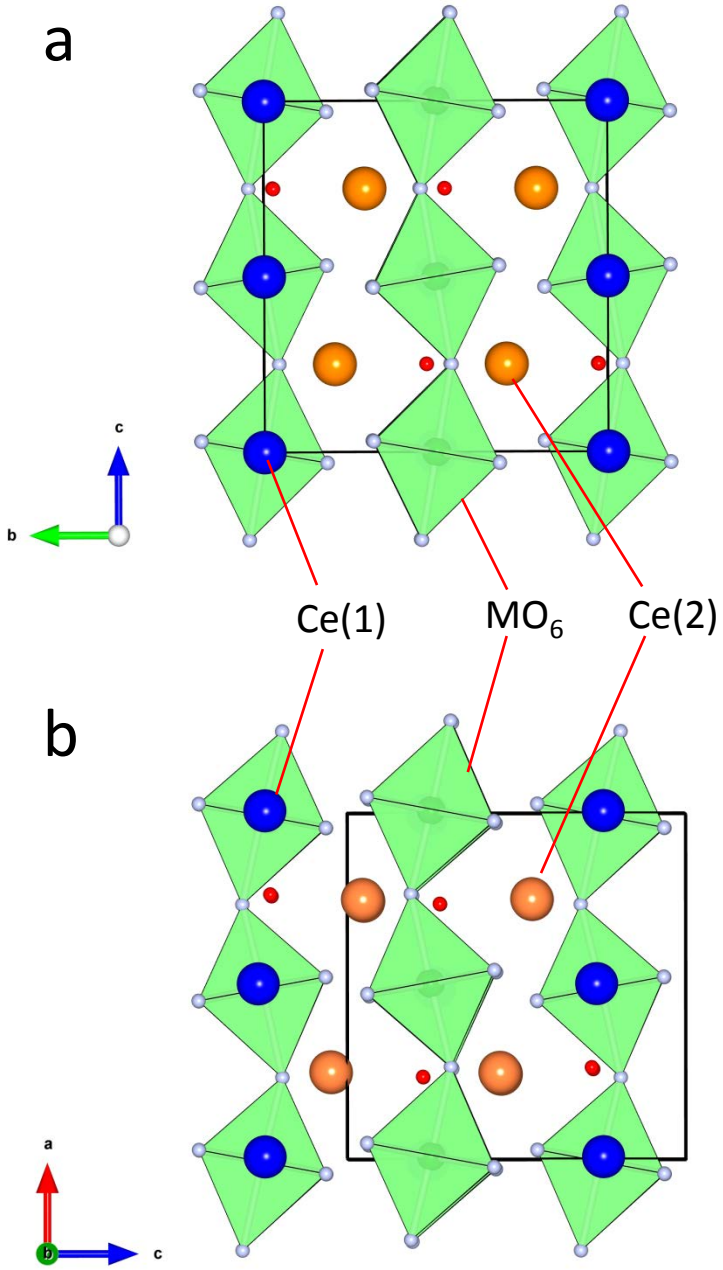


Fig. 3

a

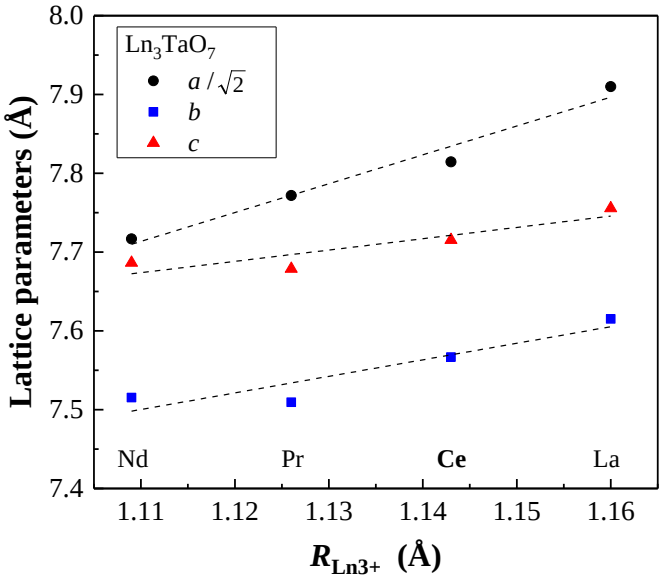
Ln3TaO7
a / √2
b
c
Lattice parameters (Å)
8.0
7.9
7.8
7.7
7.6
7.5
7.4
Nd
Pr
Ce
La
1.11
1.12
1.13
1.14
1.15
1.16
R Ln3+ (Å)

b

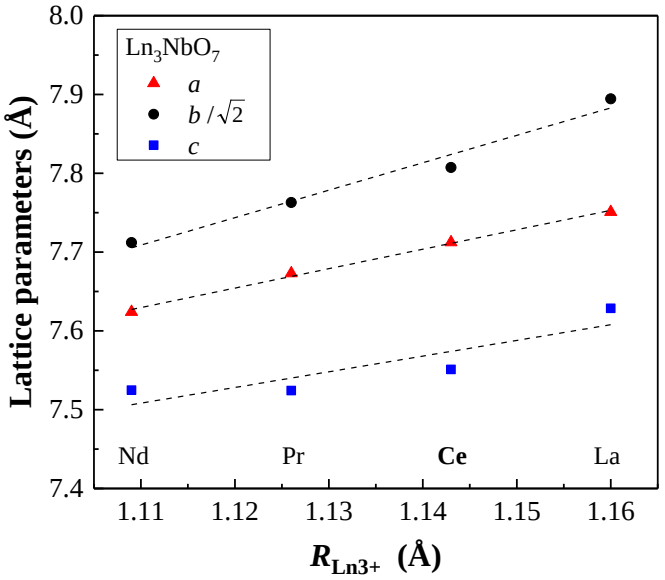
Ln3NbO7
a
b / √2
c
Lattice parameters (Å)
8.0
7.9
7.8
7.7
7.6
7.5
7.4
Nd
Pr
Ce
La
1.11
1.12
1.13
1.14
1.15
1.16
R Ln3+ (Å)

Fig.4

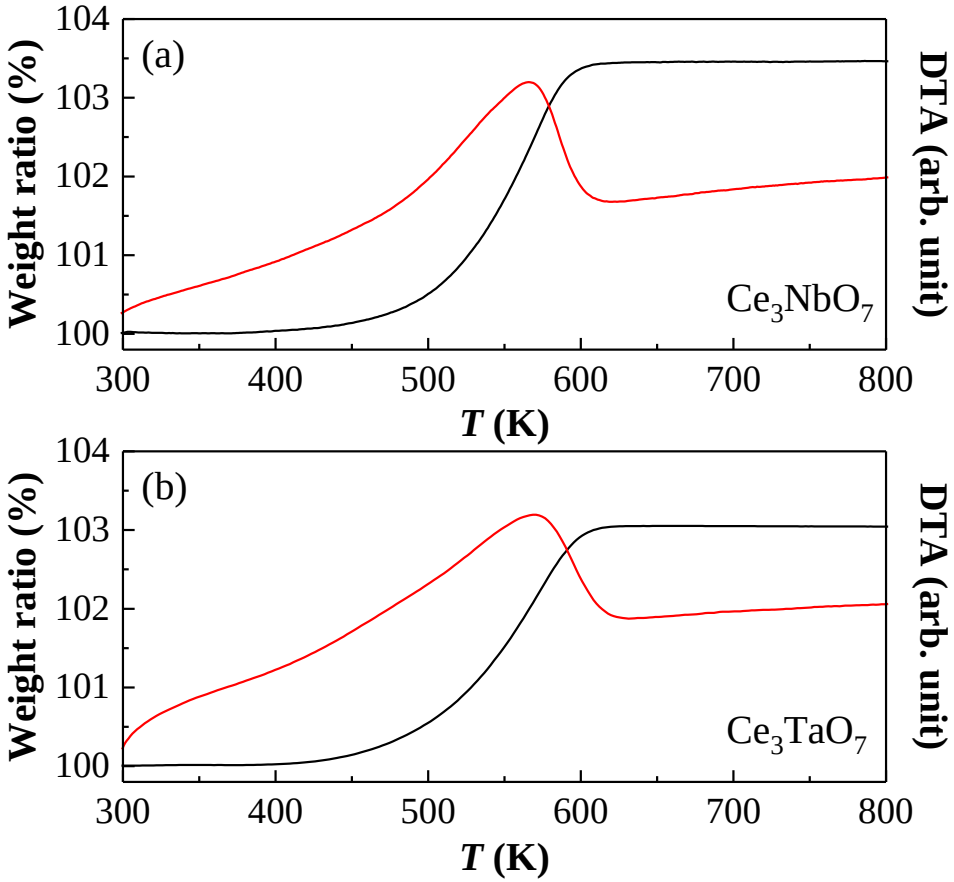
(a)
Ce3NbO7
Weight ratio (%)
DTA (arb. unit)
T (K)
104
103
102
101
100
300
400
500
600
700
800
(b)
Ce3TaO7
Weight ratio (%)
DTA (arb. unit)
T (K)

Fig. 5

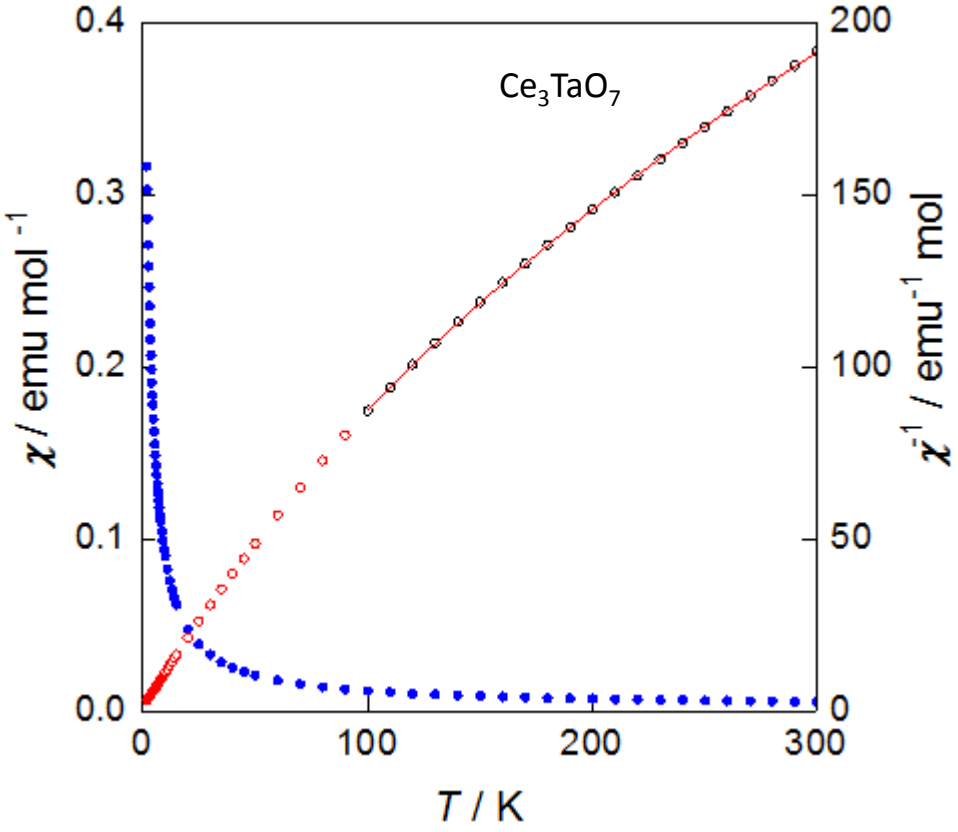
Ce3TaO7
χ / emu mol-1
χ-1 / emu-1 mol
T / K
0.4
0.3
0.2
0.1
0.0
200
150
100
50
0
0
100
200
300

Fig.6

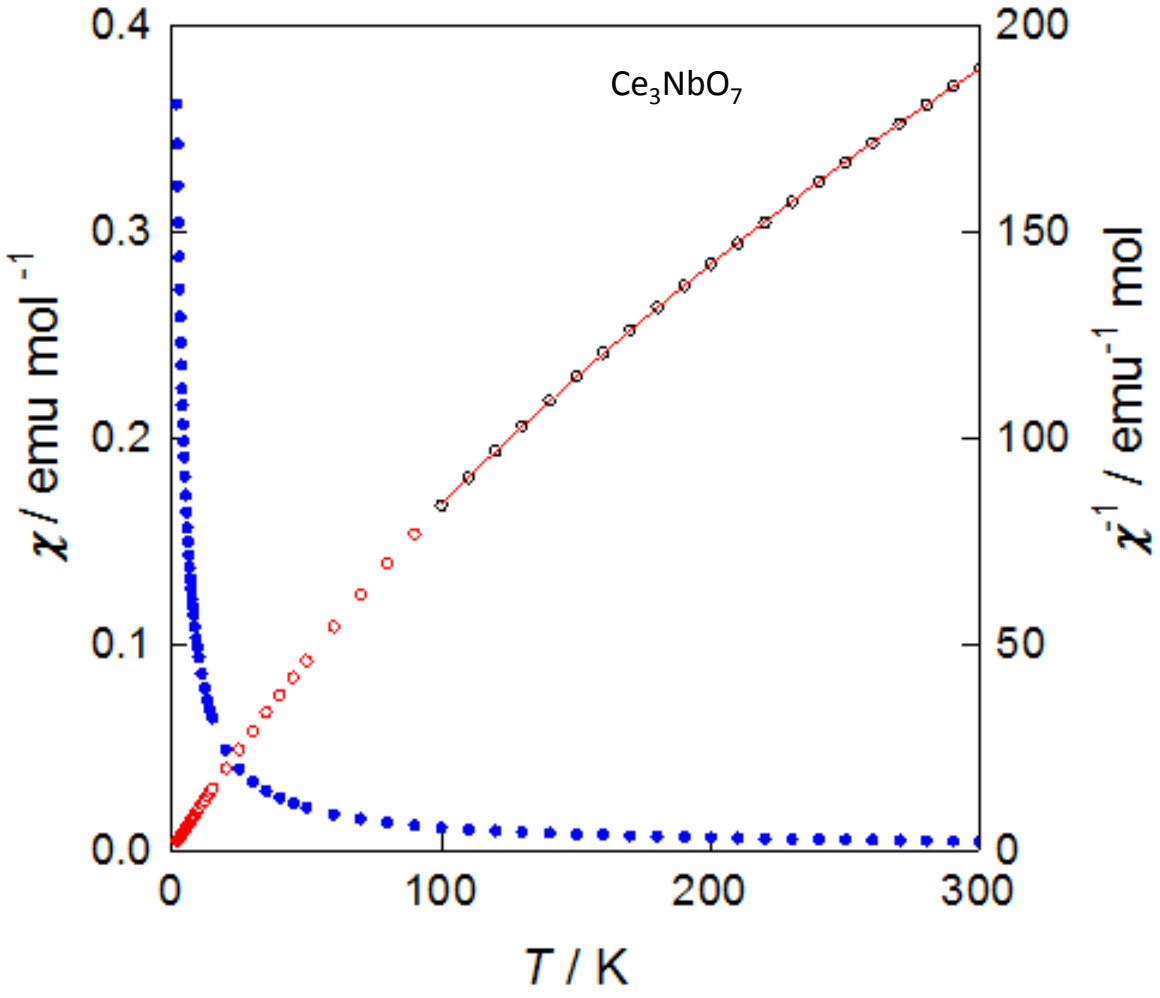
Ce3NbO7
χ / emu mol-1
χ-1 / emu-1 mol
T / K
0.0
0.1
0.2
0.3
0.4
0
50
100
150
200
0
100
200
300

Fig.7

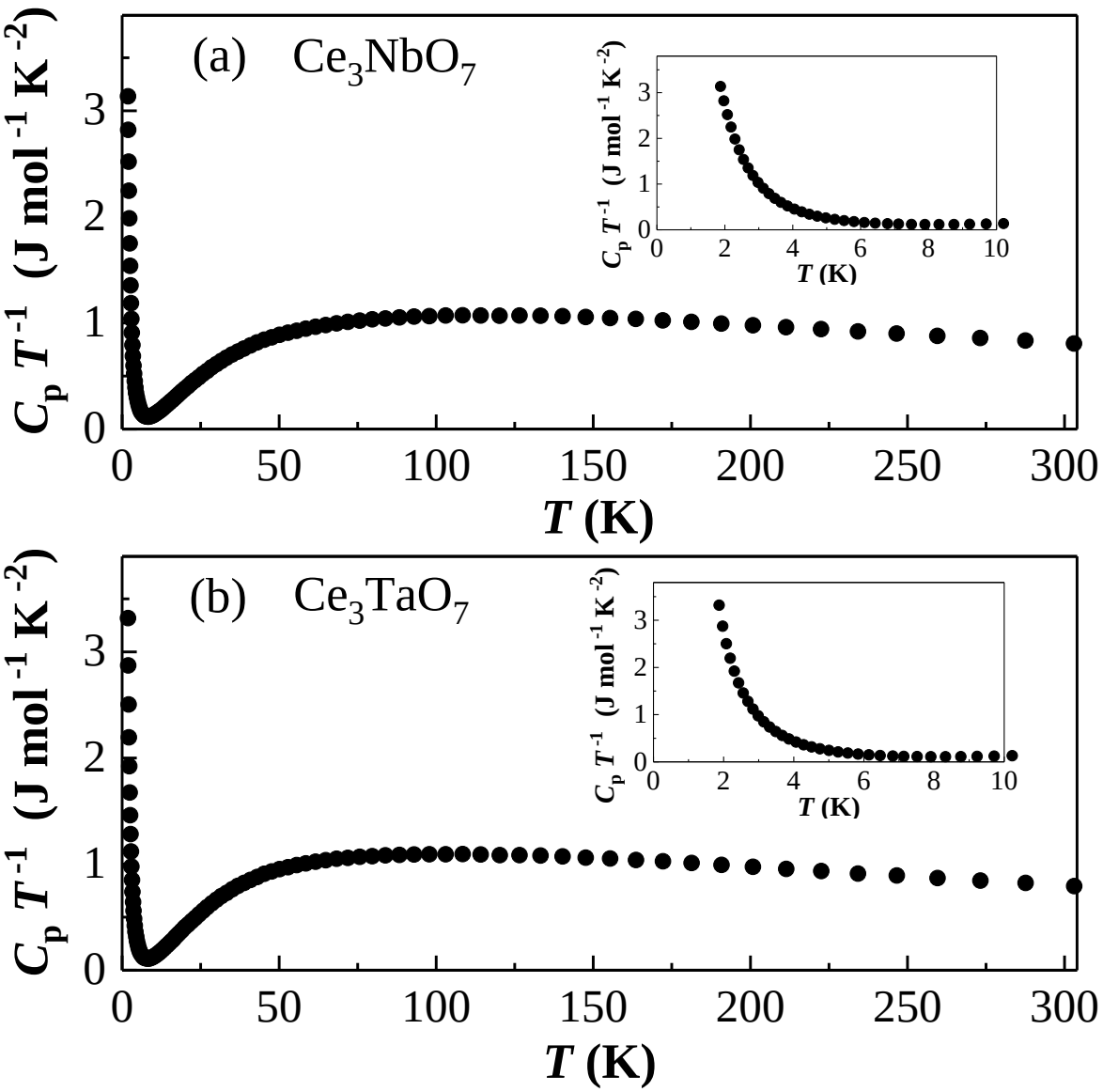


Fig.8